MRP5 and MRP9 play a concerted role in male reproduction and mitochondrial function

Ian G. Chambers[a], Praveen Kumar[b], Jens Lichtenberg[c], Pengcheng Wang[b], Jianshi Yu[b], John D. Phillips[d], Maureen A. Kane[b], David Bodine[c], and Iqbal Hamza[a,1]

[a]Department of Animal and Avian Sciences and Department of Cell Biology and Molecular Genetics, University of Maryland, College Park, MD 20742; [b]Department of Pharmaceutical Sciences, University of Maryland School of Pharmacy, Baltimore, MD 21201; [c]Genetics and Molecular Biology Branch, National Human Genome Research Institute, NIH, Bethesda, MD 20814; and [d]Department of Medicine, University of Utah School of Medicine, Salt Lake City, UT 84132

Edited by Michael Marletta, University of California, Berkeley, CA; received June 23, 2021; accepted December 21, 2021

Multidrug Resistance Proteins (MRPs) are transporters that play critical roles in cancer even though the physiological substrates of these enigmatic transporters are poorly elucidated. In *Caenorhabditis elegans*, MRP5/ABCC5 is an essential heme exporter because *mrp-5* mutants are unviable due to their inability to export heme from the intestine to extraintestinal tissues. Heme supplementation restores viability of these mutants but fails to restore male reproductive deficits. Correspondingly, cell biological studies show that MRP5 regulates heme levels in the mammalian secretory pathway even though MRP5 knockout (KO) mice do not show reproductive phenotypes. The closest homolog of MRP5 is MRP9/ABCC12, which is absent in *C. elegans*, raising the possibility that MRP9 may genetically compensate for MRP5. Here, we show that MRP5 and MRP9 double KO (DKO) mice are viable but reveal significant male reproductive deficits. Although MRP9 is highly expressed in sperm, MRP9 KO mice show reproductive phenotypes only when MRP5 is absent. Both ABCC transporters localize to mitochondrial-associated membranes, dynamic scaffolds that associate the mitochondria and endoplasmic reticulum. Consequently, DKO mice reveal abnormal sperm mitochondria with reduced mitochondrial membrane potential and fertilization rates. Metabolomics show striking differences in metabolite profiles in the DKO testes, and RNA sequencing shows significant alterations in genes related to mitochondrial function and retinoic acid metabolism. Targeted functional metabolomics reveal lower retinoic acid levels in the DKO testes and higher levels of triglycerides in the mitochondria. These findings establish a model in which MRP5 and MRP9 play a concerted role in regulating male reproductive functions and mitochondrial sufficiency.

multidrug resistance proteins | heme | mitochondria | reproduction | fertility

Multidrug Resistance Proteins (MRPs) belong to the type C subclass of the ATP Binding Cassette (ABCC) transporters, a highly conserved family of proteins that have been studied for decades for their role in cancers (1–7). MRPs are notoriously up-regulated in a number of malignancies because of their ability to efflux a wide range of synthetic and chemotherapeutic agents, conferring cancer cells resistance to drug treatments (3, 8–11). Due to their critical importance in human health and clinical outcomes, myriads of MRP substrates have now been identified, particularly from in vitro studies of tumor cell lines (3, 4, 6, 12, 13). However, the promiscuity of drugs effluxed in this context is likely a functional consequence of cancer cells hijacking these active transporters rather than that being their primary evolutionary role. Therefore, a major outstanding item remaining in the MRP field is the determination of physiological functions and substrates for a number of these transporters.

Previous work from our group shed some light on the function of one such ABCC transporter, MRP5/ABCC5, where studies in worms, yeast, zebrafish, and mammalian cells demonstrated it to be a heme exporter (14). Prior to this discovery, the role of MRP5 appeared to be that of cyclic nucleotide export from cells, as demonstrated by transport of cGMP in membrane vesicles expressing human MRP5 in vitro (12, 15). However, the generation of MRP5 null mice demonstrated little to no contribution in cGMP efflux and no observable overt phenotypes, leaving the physiological relevance of this transporter unclear outside its in vitro or cancer cell context (16, 17). This is not the case in *Caenorhabditis elegans*, a heme auxotroph, where MRP-5 is absolutely essential for intercellular heme trafficking, and knockout (KO) of *mrp*-5 results in heme deficiency and embryonic lethality (14).

While cell biological studies in mouse embryonic fibroblasts from MRP5 KO mice confirmed that MRP5 indeed plays a conserved role in heme export, i.e., transporting heme into the secretory pathway for incorporation into hemoproteins or exporting it from the cell across the plasma membrane (14, 18–20), MRP5 KO mice do not show any heme-related phenotypes in vivo. A postulated hypothesis to explain these differences could be genetic compensation by other closely related transporters, which are phylogenetically conserved in higher-order eukaryotes but absent in the *C. elegans* genome (14, 21). A candidate for this proposed compensation and further functional delineation is MRP9/ABCC12, the closest relative of MRP5 and one of the last of the ABCC proteins to have been discovered (6, 22, 23). MRP9 is highly expressed in male reproductive tissues but fails to effectively efflux drugs in vitro, and its endogenous function remains to be elucidated (6, 24, 25).

In this work, we generate MRP9 KO and MRP9/MRP5 double KO (DKO) mouse models to fully characterize these

Significance

Multidrug Resistance Proteins (MRPs) are typically implicated in cancer biology. Here, we show that MRP9 and MRP5 localize to mitochondrial-associated membranes and play a concerted role in maintaining mitochondrial homeostasis and male reproductive fitness. Our work fills in significant gaps in our understanding of MRP9 and MRP5 with wider implications in male fertility. It is plausible that variants in these transporters are associated with male reproductive dysfunction.

Author contributions: I.G.C., P.K., D.B., and I.H. designed research; I.G.C., P.K., P.W., J.Y., J.D.P., M.A.K., and I.H. performed research; I.G.C., P.K., J.L., J.D.P., M.A.K., D.B., and I.H. contributed new reagents/analytic tools; I.G.C., P.K., J.L., P.W., J.Y., J.D.P., M.A.K., D.B., and I.H. analyzed data; and I.G.C. and I.H. wrote the paper.

Competing interest statement: I.H. is the President and Founder of Rakta Therapeutics Inc. (College Park, MD), a company involved in the development of heme transporter-related diagnostics.

This article is a PNAS Direct Submission.

[1]To whom correspondence may be addressed. Email: hamza@umd.edu.

This article contains supporting information online at http://www.pnas.org/lookup/suppl/doi:10.1073/pnas.2111617119/-/DCSupplemental.

Published February 4, 2022.

transporters' physiological functions. Loss of MRP9 and MRP5 disrupts mitochondrial homeostasis and regulatory pathways in the testes, with RNA sequencing (RNAseq) and metabolomic analyses revealing large-scale perturbation in genes and metabolism related to mitochondrial function. Together, these results establish a concerted and critical role for MRP9 and MRP5 in male reproduction and mitochondrial metabolism, implying that the ancestral role of MRP5 in *C. elegans* reproduction was co-opted in the vertebrate ancestor.

Results

Loss of MRP9 in Mice Induces the Expression of MRP5 in the Testes. *C. elegans mrp-5(ok2067)* deletion mutants display lethality unless rescued with dietary heme supplementation (14). Serendipitously, we found that even in the presence of heme *mrp-5(ok2067)*, male worms are defective in mating (*SI Appendix*, Fig. S1 *A* and *B*). These worms exhibit defective mating apparatus with stunted tail fan formation, reduced numbers of rays, and spicules that fail to retract despite normal mating behaviors. Given that hermaphrodite *mrp-5* KO worms mate normally with wild-type (WT) males, it would appear the defect is paternal. For these reasons, we hypothesized that MRP-5 may have additional functions related to male reproduction outside of its traditional role in heme transport and homeostasis. MRP5 KO mice, however, show no reproductive deficiencies, prompting inquiry into other ABCC transporters that may genetically compensate for the loss of MRP5 in higher-order vertebrates.

Phylogenetic analysis of ABCC transporters across metazoans confirmed that members of the short MRP clade (ABCCs: 4, 5, 7, 11, 12) cluster tightly together across species, indicating their evolutionary relation (6, 14). Within this subclade, *C. elegans* has only MRP-5, whereas most vertebrates have an additional paralog, MRP9 (Fig. 1*A*), which is conserved in all higher-order vertebrates but remains to be fully characterized in vivo. We therefore generated MRP9 mutant mice via CRISPR/Cas9 to explore MRP9's endogenous functions. Utilizing guide RNAs targeted to the second exon of *Abcc12*, we were able to generate 11 founder animals with various indels at the target site, and a 17 bp insertion line was selected for further characterization (Fig. 1*B* and *SI Appendix*, Fig. S1*C*). RT-PCR confirmed that the frameshift-inducing mutation was present with no alternate start sites or splice variants identified (*SI Appendix*, Fig. S1*D*).

Abcc12$^{-/-}$ animals are viable and reach adulthood with no overt phenotypes. Immunoblots of lysates from testes of adult mice confirmed no detectable MRP9 protein in KO animals

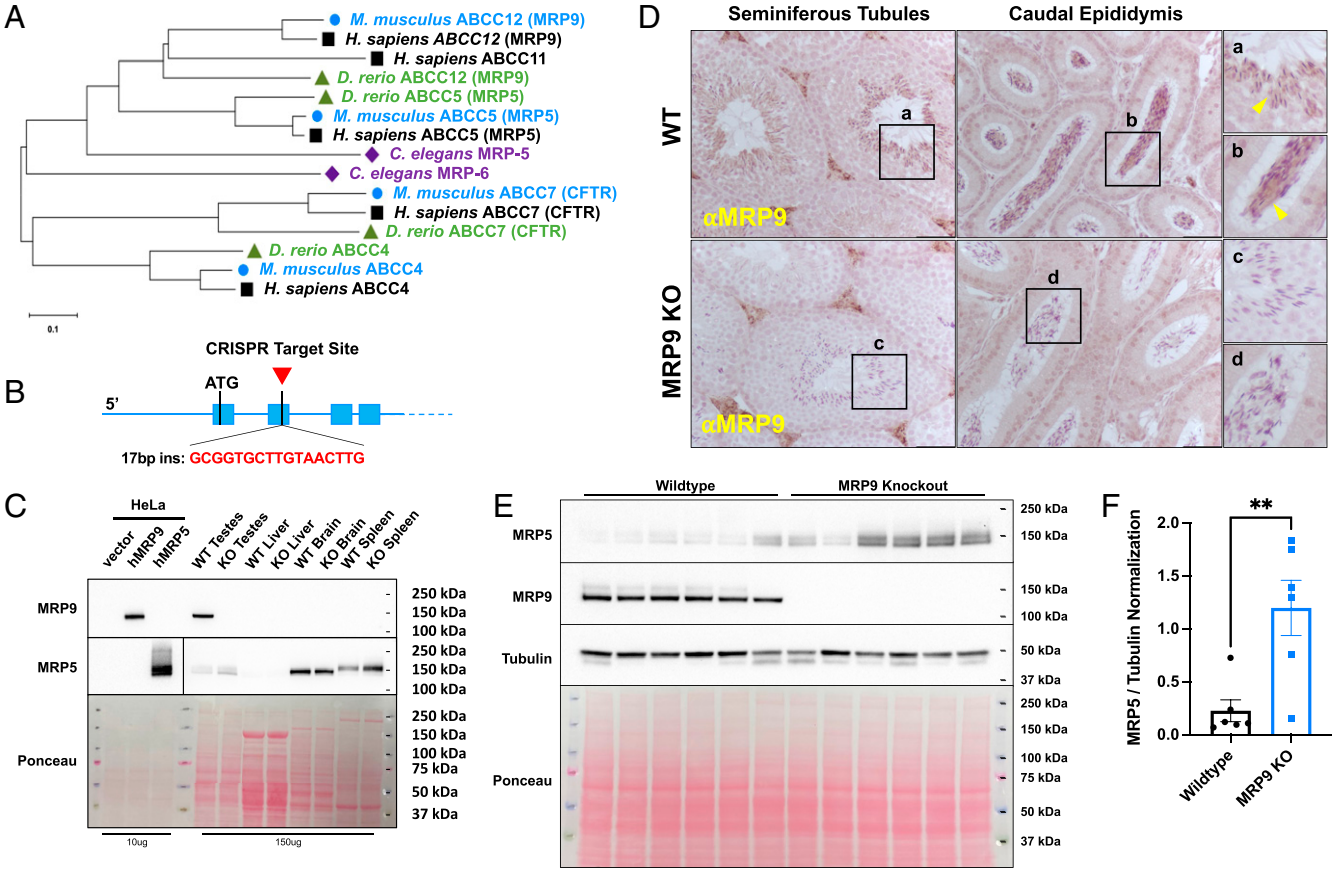

Fig. 1. Ablation of MRP9 in mice induces MRP5 expression in the testes. (*A*) Amino acid FASTA sequences for MRPs in humans, mice, zebrafish, and worms were aligned and used to generate the optimal phylogenetic tree shown. The evolutionary history was inferred using the Neighbor-Joining method. The tree is drawn to scale, with branch lengths in the same units as those of the evolutionary distances used to infer the phylogenetic tree. The evolutionary distances were computed using the Poisson correction method and are in the units of the number of amino acid substitutions per site. (*B*) Gene loci schematic of 5′ UTR and the first four exons of *Abcc12* indicating the CRISPR target site in second exon for the generation of KO MRP9 mice. (*C*) Immunoblot of protein lysates from transfected HeLa cells and WT and MRP9 KO tissues probed for MRP9 and MRP5. (*D*) MRP9 immunohistochemistry analysis of paraffin-embedded testes tissue sections from WT and MRP9 KO mice. Tissue sections were probed for MRP9 and lightly counterstained with hematoxylin. Images are representative of at least three mice. (Scale bar: 100 μm.) (*E*) Immunoblot of protein lysates from WT and MRP9 KO testes (n = 6) probed for MRP5, MRP9, and Tubulin. (*F*) Quantification of MRP5 protein expression in WT and MRP9 KO testes from *E*, normalized to Tubulin; P value = 0.0061.

(Fig. 1*C*). Immunohistochemistry of tissue sections showed MRP9 in both the maturing and developed spermatozoa of seminiferous tubules and caudal epididymis, respectively, consistent with the findings reported by Ono et al. (Fig. 1*D*) (24). Recent single cell RNAseq datasets of the testis niche further confirmed these findings, as the gene expression profile of *Abcc12* is distinctly germ cell specific (*SI Appendix*, Fig. S1*E*) (26). This is in contrast to *Abcc5*, which appears to be normally expressed in early spermatogonia precursors as well as Sertoli and Leydig cells (*SI Appendix*, Fig. S1*E*). Immunoblotting of lysates from additional tissues of WT and KO mice revealed the testes as the only organ with any appreciable amounts of both MRP9 and MRP5 (Fig. 1*C*). Importantly, MRP9 KO testes showed elevated levels of MRP5, raising the notion that MRP5 could be compensating for MRP9 deficiency in the testes (Fig. 1 *E* and *F*).

MRP9 and MRP5 Are Required for Male Reproductive Fitness. MRP9 KO mice do not show any statistically significant defects in reproduction, with expected litter sizes and normal Mendelian F1 segregation when intercrossed ($n = 166$, $\chi^2 = 0.976$, P value = 0.614) (Fig. 2*A*). MRP9 KO crossed to MRP5 KO mice successfully generated DKO mice that reached adulthood with no overt phenotypes. Although DKO mice were viable, they were deficient in their reproductive capacity; the average number of pups from intercrosses of DKO mice were significantly reduced compared to WT ($n > 33$ litters, P value < 0.0001) (Fig. 2*B*). Interestingly, fecundity was restored back to single KO levels when DKO females were crossed with WT or double heterozygous males alone, suggestive that the failure may be paternal ($n > 21$ litters, P value < 0.0001) (Fig. 2*B*). Furthermore, DKO male mice set up to breed had high incidences of penile prolapse and clogging of their urogenital tracts with seminal coagulum (five DKOs compared to zero WT male mice), regardless of the female genotype (Fig. 2*C*). These findings, taken together with our protein expression data, prompted a closer investigation into male fitness as the major defect behind the DKO reproductive failure. Indeed, sperm from DKO mice had significantly lower in vitro fertilization (IVF) rates compared to WT (Fig. 2*D*). Interestingly, this may be attributed to sperm fitness/quality rather than quantity, as DKO sperm showed trends of decreased motility with no differences in total sperm production (*SI Appendix*, Fig. S2 *A* and *B* and Fig. 2*E*).

MRP9 Is Localized to Mitochondrial-Associated Membranes in the Testes. To understand why DKO male mice have reduced fecundity and sperm fitness, we further characterized the function of these proteins in this context. Given their distinct spatiotemporal gene expressions (*SI Appendix*, Fig. S1*E*), we hypothesized that these MRPs may play overlapping subcellular roles during spermatid maturation. The Borst group had shown that MRP9 is localized to the sperm midpiece (24, 27, 28), and, when expressed in HEK293, closely resembled an ER localization (24). In polarized MDCKII cells, transfection of *ABCC12* showed a distinct intracellular distribution of MRP9 in stark contrast to MRP5, which localized primarily to the basolateral surface of the plasma membrane (Fig. 3*A*). To determine if this was also the case in vivo or merely a consequence of ectopic expression, we performed subcellular fractionation of lysates from mouse testes. Immunoblotting showed that MRP9 protein was actually significantly enriched in 9,000 × *g* fractions that pellet mitochondria (Fig. 3*B*). This result was surprising given previously published findings (24, 29, 30) and that MRP9 lacks any obvious mitochondrial targeting sequences. However, an explanation for this unexpected result could be that mitochondrial-associated membranes (MAMs), the

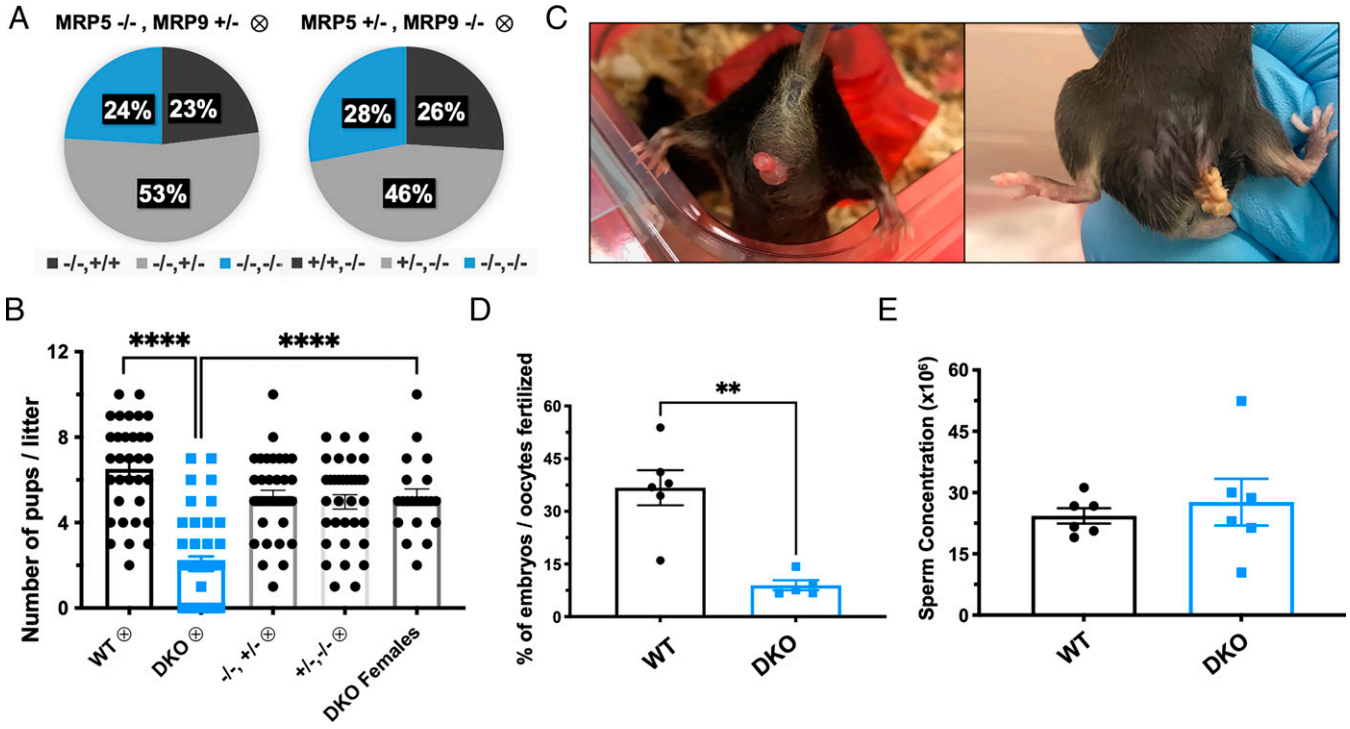

Fig. 2. DKO mice are viable but have reduced male reproductive fecundity. (*A*) Genotyped progeny from MRP5$^{-/-}$ and MRP9$^{+/-}$ intercrosses (*Left*), $n = 190$, $\chi^2 = 0.568$, and P value = 0.753; genotyped progeny from MRP5$^{+/-}$ and MRP9$^{-/-}$ intercrosses (*Right*), $n = 166$, $\chi^2 = 0.976$, and P value = 0.614. (*B*) Quantification of the number of pups weaned per litter of intercrossed WT, DKO, MRP5$^{-/-}$ MRP9$^{+/-}$, MRP5$^{+/-}$ MRP9$^{-/-}$, and DKO females crossed with WT or double het mice, ****P value < 0.0001. (*C*) Representative images of penile prolapse (*Left*) and expressed seminal coagulum (*Right*) in DKO male mice set up for breeding. (*D*) IVF rate of WT and DKO sperm incubated with WT oocytes for 5 h at a concentration of 1.0×10^6 sperm/mL. The next day, total number of two cell embryos were determined, and fertilization rate was calculated based on dividing by the total number of oocytes inseminated for each male; **P value = 0.0019. (*E*) Total concentration of spermatozoa calculated by Integrated Visual Optical System (IVOS) computer-assisted sperm analyzer.

contact sites of the ER that are intimately associated with the mitochondria, are enriched in our crude mitochondrial fractions (31–34).

Next, we performed Airyscan super-resolution microscopy on HeLa cells transiently transfected with human *ABCC12* (Fig. 3*C*). Three-dimensional (3D) rendering revealed that MRP9 was in close proximity or at the interface of the mitochondria (Mitotracker) and ER (Calnexin) (Fig. 3*C* and Movie S1). To validate this localization, we performed Percoll-based differential centrifugations to further separate crude mitochondrial fractions into purified mitochondria and MAMs from testes tissue homogenates (32). Immunoblots of distinct testes fractions revealed that MRP9 was in fact not present in purified mitochondria but significantly enriched in MAMs, characterized by the markers Mitofusin 2 and Calnexin (Fig. 3*D*). Interestingly, probing for MRP5 from these same fractions indicated that it too was enriched in the MAMs as well as total membranes (Fig. 3*E*). These results indicate that subcellular expression patterns of MRPs may vary dependent on tissue contexts.

Multiomics of DKO Testes Reveals Extensive Perturbation and Mitochondrial Dysfunction. In order to systematically dissect why the combined loss of MRP9 and MRP5 manifests in male reproductive dysfunction, we sought to understand what substrates may be transported by these proteins and how their absence may impact homeostatic pathways in the testes. To achieve this, we performed untargeted metabolomics and RNAseq from paired testes of the same mice to integrate any differential metabolites and gene expression changes (*SI Appendix*, Fig. S3*A*). Global untargeted metabolomics of testes indicated significant perturbation, with 24 of the top 25 differential species measured from negative ion mode acquisition of aqueous phase metabolites showing accumulation in the DKO (Fig. 4*A*). Dramatic differences in metabolite profiles were evident however regardless of the extraction method (aqueous vs. organic) or the ion mode of acquisition (negative vs. positive) (*SI Appendix*, Fig. S3 *B* and *C*). Analysis of these data allowed for the identification of mass-to-charge ratios (*m*/*z*) of hyperaccumulated candidate metabolites. However, given that our sampling was untargeted, a particular *m*/*z* could represent multiple possibilities of actual biological compounds even given the high mass accuracy and resolution of the Q-TOF (quadrupole - time of flight) platform. As a means to associate these putative species with specific metabolites, all significant *m*/*z*s identified from our six untargeted datasets were pooled and processed using MetaboAnalyst Mummichog analyses (35). From the species of interest analyzed, 65 metabolites were assigned possible Kyoto Encyclopedia of Genes and Genomes (KEGG) IDs (*SI Appendix*, Table S1). Among these, succinyl-CoA, which is also an essential TCA cycle energy source and a heme precursor, had the largest fold change increase in DKO testes (36, 37).

RNAseq analysis from the same tissues found 3,736 differentially expressed genes between WT and DKO, with a number of top

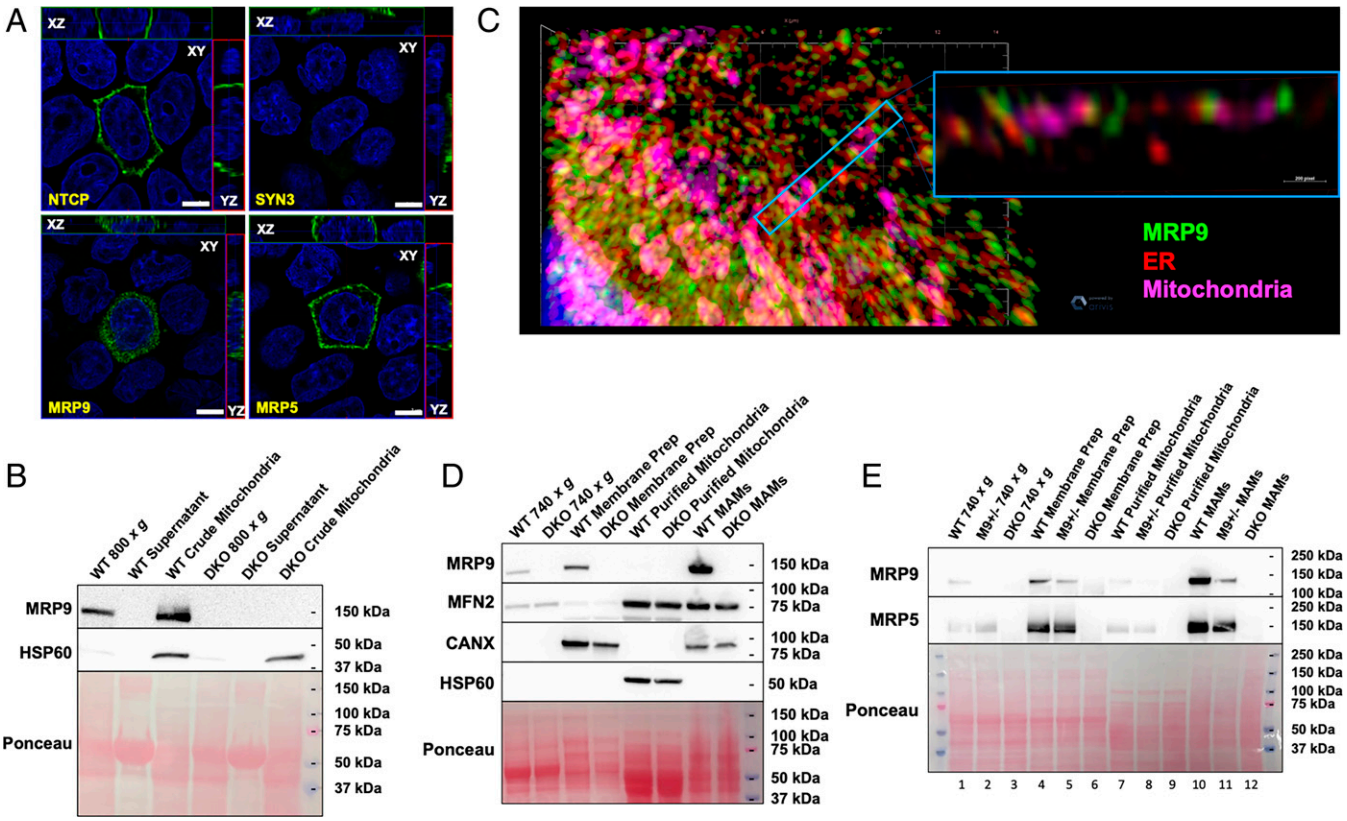

Fig. 3. MRP9 is enriched in MAMs of the testes. (*A*) MDCKII cells grown on transwell filters transfected with basolateral marker sodium taurocholate cotransporting polypeptide *NTCP-GFP*, apical marker syntaxin 3 *SYN3-GFP*, *ABCC12*, or *ABCC5*. Polarization of the monolayers was additionally confirmed prior to fixation by measurement of transepithelial electrical resistance. A representative confocal section (XY) is depicted along with the composite stacks in the side panel views (XZ and YZ). (Scale bar: 5 μm.) (*B*) Immunoblot analysis of crude mitochondrial fractionation from testes of mice. Membrane was probed for MRP9 and HSP60, a mitochondrial matrix protein marker. (*C*) Airyscan super-resolution microscopy and 3D rendering of HeLa cells transfected with human *ABCC12* for 48 h and treated with Mitotracker Deep Red FM immediately prior to fixation and immunofluorescence. Antibody probing for MRP9 and Calnexin was followed by Alexa-488 and Alexa-568 secondary antibodies, respectively, followed by DAPI counter staining prior to mounting. (*D*) Immunoblot analysis of subcellular fractionation from testes of mice. Membranes were probed for MRP9 (M9II-3 antibody) and MFN2, CANX, and HSP60 markers of outer mitochondrial membrane, ER membrane, and mitochondrial matrix, respectively. (*E*) Immunoblot of subcellular fractionation from testes of WT, MRP9 heterozygous, and DKO mice. Membranes were probed for MRP9 (M9I-27 antibody) and MRP5.

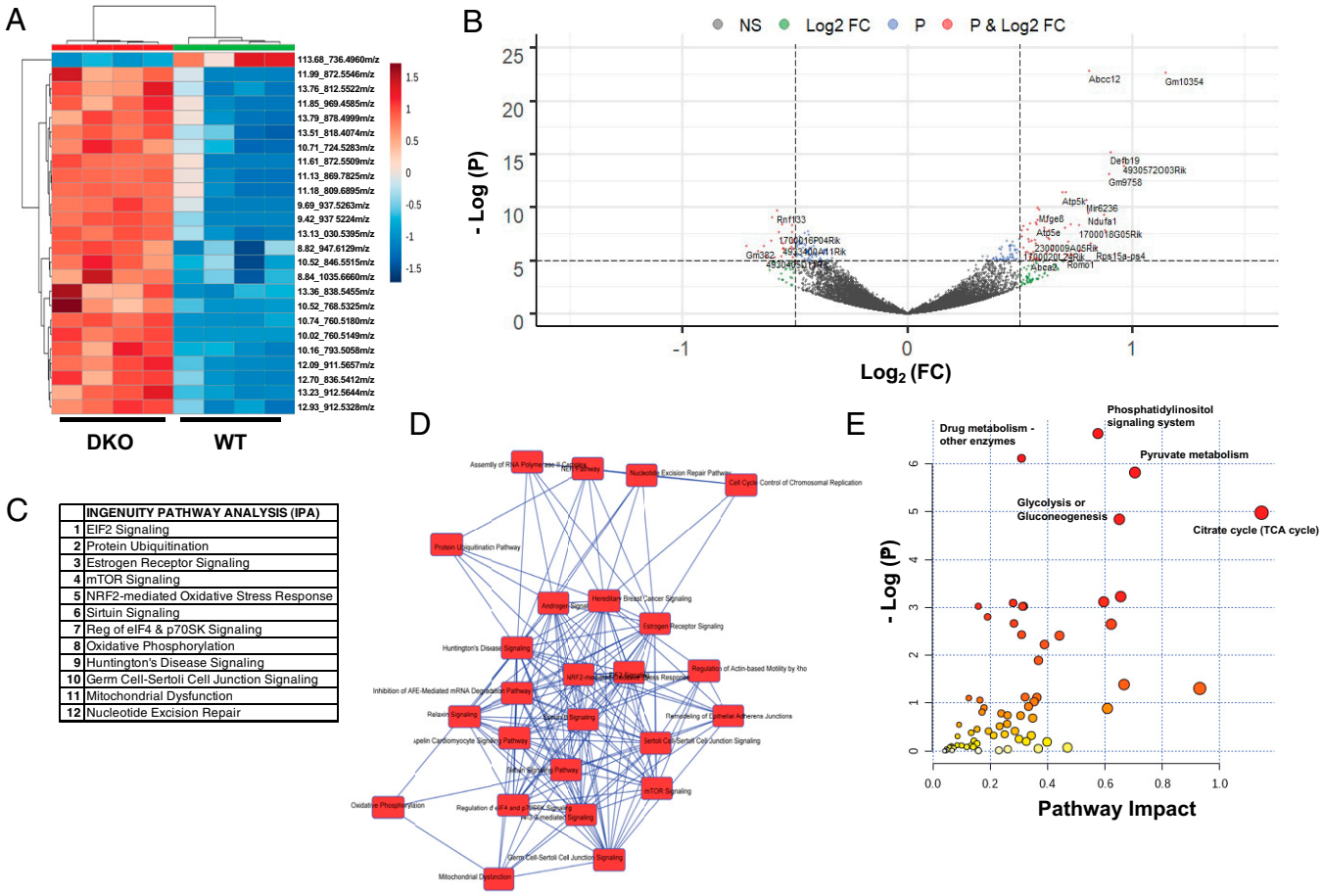

	INGENUITY PATHWAY ANALYSIS (IPA)
1	EIF2 Signaling
2	Protein Ubiquitination
3	Estrogen Receptor Signaling
4	mTOR Signaling
5	NRF2-mediated Oxidative Stress Response
6	Sirtuin Signaling
7	Reg of eIF4 & p70SK Signaling
8	Oxidative Phosphorylation
9	Huntington's Disease Signaling
10	Germ Cell-Sertoli Cell Junction Signaling
11	Mitochondrial Dysfunction
12	Nucleotide Excision Repair

Fig. 4. Metabolomics and transcriptomics reveal pervasive perturbation in DKO testes. (*A*) VIP heatmap of the top 25 differential metabolites in testes from aqueous phase extractions on C18 column run in negative mode. (*B*) Volcano plot of gene expression changes from DKO and WT testes; significance threshold set at $-\log(P \text{ value}) > 5$. (*C*) Top 12 GO pathways perturbed in DKO testes based on Qiagen IPA analysis. (*D*) Key overlapping canonical pathways in testes based on Qiagen IPA analysis. (*E*) MetaboAnalyst pathway impact analysis from combining RNAseq differential gene expression changes and metabolomics mummichog putative KEGG IDs of the testes; top five pathways by *P* value are annotated.

genes differentially expressed, including uncharacterized and testis-specific predicted genes (*Gm10354*, *Gm9758*, *5430401F13Rik*) as well as mitochondrial respiratory genes (*Atp5k*, *Ndufa1*, *Atp5e*) (Fig. 4*B*). To unbiasedly determine the pathways and Gene Ontology (GO) terms most significantly affected in these mice we performed Ingenuity Pathway Analysis (IPA) (Fig. 4*C* and *SI Appendix*, Fig. S3*D*). The majority of the top GO canonical pathways identified by IPA were intimately interconnected and overlapped with mitochondrial function (Fig. 4 *C* and *D*). Of note, the top two pathways identified, EIF2 Signaling and Protein Ubiquitination, are critical for mitigating unfolded protein response (UPR) and mitochondrial dysfunction associated with iron and heme deficiencies (38).

To generate metabolite-gene relationships, we integrated our metabolomics and RNAseq data using MetaboAnalyst Joint Pathway Analysis. The merged data analysis revealed significant mitochondrial pathway dysfunction with energy production components of the cell (TCA Cycle, Pyruvate Metabolism, and Glycolysis) showing the highest impact (Fig. 4*E*). Taken together, these findings reinforce a role for MRP9 and MRP5 in mitochondrial metabolism in the testes.

EIF2a Phosphorylation and Associated Signaling Pathways Mitigate Mitochondrial Dysfunction. Having identified mitochondrial dysfunction as the overarching factor from our integrative analysis, we sought to determine the specific mechanisms that underlie this dysfunction in the testes. Mining our RNAseq dataset, we built an analysis pipeline to determine and curate fold changes of all genes associated with a given pathway from published GO databases for downstream investigation and mapping. In querying all genes associated with the mitochondria and mitochondrial dysfunction, we identified over 200 dysregulated genes (Fig. 5*A*). We then asked what individual genes or pathways may be involved in responding to such a significant level of disruption. Given that the top-related pathway identified from our IPA studies was EIF2 signaling, we investigated all associated genes and found 95 that were perturbed in DKO testes (Fig. 5*B*). EIF2 signaling and EIF2a phosphorylation by the heme responsive kinase HRI (*Eif2ak1*) are established mechanisms for regulating translation to reduce mitochondrial stress and UPR in situations of intracellular heme deficiency (38–41). In particular, this model is well documented in the erythron, where heme is critical, as it becomes the limiting factor for incorporation into hemoglobin for red blood cell differentiation (*SI Appendix*, Fig. S4*A*). Limited studies have characterized a similar role in mitigating mitochondrial dysfunction in neurons, but very little is known about HRI and EIF2a signaling in other tissues such as the testes (39, 42–45). Indeed, analysis of the testes single cell RNAseq dataset determined that both factors are expressed during spermatid maturation (*SI Appendix*, Fig. S4*B*), and immunoblotting of total testes homogenates confirmed significant EIF2a protein expression (Fig. 5*C*) (26).

Importantly, EIF2a phosphorylation was significantly increased in the DKO mice, implicating the involvement of the EIF2a pathway in mitigating potential responses to UPR and mitochondrial dysfunction in the testes (Fig. 5 *C* and *D*). We next asked if the observed EIF2 signaling in the testes of DKO mice was in response to heme deficiency, as is the hallmark in the erythron. If so, one would expect that iron/heme homeostasis should also be perturbed in the testes of these mice. Subsequent probing with our pipeline pathway revealed heme and iron homeostasis related genes were in fact significantly altered (*SI Appendix*, Fig. S4*C*). To determine if heme levels themselves were also impacted, we measured total heme in male reproductive tissues. Heme levels in the caudal epididymides, the storage sites for mature sperm, showed a significant decrease (Fig. 5*E*), while whole testes and seminal vesicles showed no differences (*SI Appendix*, Fig. S4 *D* and *E*). These results suggest that there is insufficient heme specifically in spermatozoa of DKO mice.

A critical component of the canonical EIF2 signaling cascade for maintaining mitochondrial function and redox homeostasis is the alteration of mTOR signaling to inhibit proliferation and enable differentiation (38, 46). Indeed, the mTOR signaling pathway was one of the most significant GO terms identified by IPA (Fig. 4*C* and *SI Appendix*, Fig. S3*D*), which we also validated with our analysis pipeline (*SI Appendix*, Fig. S5*A*). Up-regulation of EIF-4E, a highly abundant translation regulation factor in the testes, has been shown to play an important role in spermatogenesis through regulation of capping stage-specific mRNAs during germ cell development (47). A modulator of these related pathways is retinoic acid, which has been implicated in mTOR/EIF-4E cascade and plays a key role in a variety of biological contexts including regulation of genes impacting mitochondrial function (48–52). Principal targets of retinoic acid include key OxPhos and respiratory genes such as NADH dehydrogenase subunits, cytochrome *c* oxidases, and the ATPases, some of the top differentially expressed genes from our RNAseq (Fig. 4*B*) (51, 53). Investigation of retinoic acid–related genes revealed significant perturbation, including decreases in the cytosolic chaperone *Crabp1*, responsible for delivering retinoic acid for catabolism, as well as binding receptors (RAR, RXRs), suggestive of dysregulated retinoic acid homeostasis (*SI Appendix*, Fig. S5*B*) (54–56). Importantly, retinoic acid signaling is essential for male germ cell differentiation, exerting key control over meiotic initiation and spermatogenesis, with defects in retinoid homeostasis a well-established cause of male infertility (57–60). Taken together, we hypothesized that retinoic acid homeostasis/signaling may play an important role in the phenotypes observed in our DKO mice. Quantification of the major components of the retinoid pathway revealed that total levels of vitamin A (retinol) and storage esters were not perturbed in the testes (*SI Appendix*, Fig. S5 *C* and *D*), but all-*trans* retinoic acid levels were significantly reduced DKOs compared to WT (*SI Appendix*, Fig. S5*E*).

To further validate if retinoic acid binding transcription factors and cascade regulators were indeed impacting mitochondrial genes of interest, we performed unbiased motif discovery on regulatory sequences of all up-regulated and down-regulated genes from our pathway pipeline (Fig. 5*A* and *SI Appendix*, Fig. S5*F*). The top five statistically significant DNA

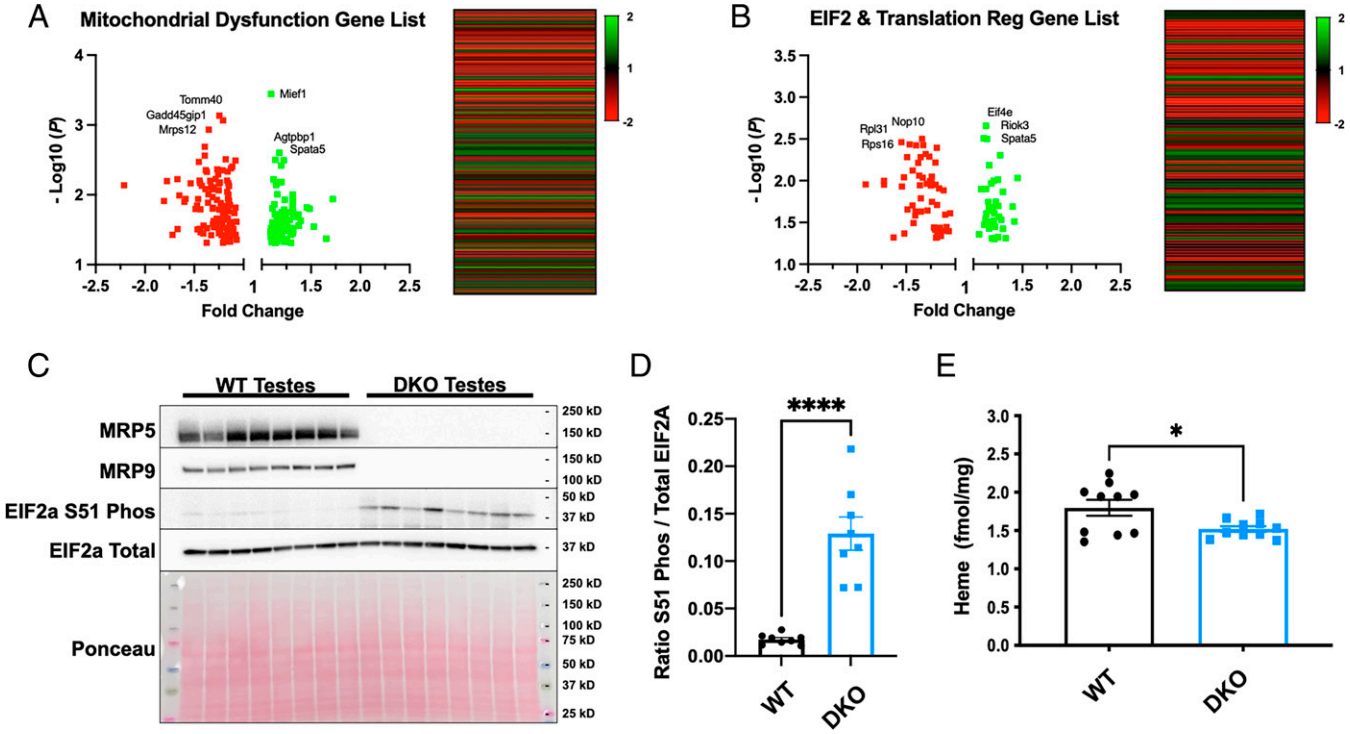

Fig. 5. Loss of MRP5 and MRP9 induces EIF2 signaling to mitigate mitochondrial dysfunction. (*A*) Output of pathway pipeline analysis investigating all "mitochondria" and "mitochondrial disfunction" GO pathway gene lists. Gene lists were curated for integration with RNA expression data. Real expression was validated by thresholding a minimum 10 TPM and statistically significant genes ($P < 0.05$) fold change were output in volcano plot and heatmap with 200 total genes identified, sorted by ascending *P* value. (*B*) Output of pathway pipeline analysis investigating all "EIF2 signaling" and "translational regulation" GO pathway gene lists. Gene lists were curated for integration with RNA expression data. Real expression was validated by thresholding a minimum 10 TPM and statistically significant genes ($P < 0.05$) fold change were output in volcano plot and heatmap with 95 total genes identified, sorted by ascending *P* value. (*C*) Immunoblot analysis of testes lysates from DKO and WT mice probed for MRP5, MRP9, Serine 51 phosphorylated EIF2a, and total EIF2a protein. Blot is representative of three separate experiments; each lane represents an individual mouse; $n = 8$ mice per genotype. (*D*) Quantification of DKO and WT phosphorylated EIF2a normalized to total EIF2a protein in *C*, ****P value < 0.0001. (*E*) Heme content of pooled caudal epididymides from DKO and WT mice by oxalic acid quantification, $n = 15$ animals per genotype (1.5 mice or 3 epididymides per replicate), *P value $= 0.0275$.

sequences identified were further analyzed and queried against known binding motifs. With two independent analysis platforms (MEME suite and HOMER), we identified significant enrichment of conserved retinoic acid–related binding motifs including putative RXRs and RORA binding sequences (*SI Appendix*, Fig. S5*F*) (61). These findings suggest a mechanistic link between transcripts related to mitochondrial dysfunction, retinoid signaling genes, and decreased retinoic acid levels, corresponding with a specific enrichment of retinoic acid binding motifs in the DKO mice.

Ablation of MRP9 and MRP5 Significantly Damages Sperm Mitochondria. To determine whether mitochondrial disruption could be related to the gene expression and metabolomic changes that are affecting sperm fertilization in the DKO testes, we analyzed mitochondria oxidative phosphorylation complexes in total testes lysates. However, all five complexes appeared to be normal and unchanged in DKOs (*SI Appendix*, Fig. S6*A*). We next fractionated the testes and performed high-throughput targeted metabolomics on each isolated fraction, allowing for the identification and quantification of specific metabolites within each subcellular niche (*SI Appendix*, Fig. S6*B*). We found that the mitochondria and MAM fractions of the DKO testes hyperaccumulate triglycerides, indicative of mitochondrial metabolism dysfunction (*SI Appendix*, Fig. S6 *C* and *D*) (62, 63).

Mature caudal epididymal sperm were then collected from WT and DKO adult mice by swim-out for mitochondrial membrane potential ($\Delta\Psi_M$) analysis and transmission electron microscopy (TEM). Staining of sperm with JC-1 revealed that DKO mice have reduced J aggregates and $\Delta\Psi_M$ compared to WT (Fig. 6 *A* and *B* and *SI Appendix*, Fig. S7*A*). Strikingly, TEM cross sections of sperm midpieces revealed DKO mice also have highly vacuolated and aberrant mitochondria, in contrast to the ubiquitously electron dense cristae in the WT (Fig. 6*C*). These defects were not observed in the single KOs or double heterozygous animals (*SI Appendix*, Fig. S7*B*).

Discussion

ABCC proteins are one of the most well-studied class of transporters due to their critical roles in cancer biology, multidrug resistance, and associated human diseases (3, 64–67). Taken together, our studies fill significant gaps in our understanding of not only of MRP9 but also MRP5, uncovering endogenous functions related to reproduction. Given MRP5 is genetically dispensable in the mouse model with low gene expression in male reproductive tissues, no studies have examined its protein levels or function in the testes (14, 15, 68, 69). Klein et al. showed a weak MRP5 signal in Leydig cells of rats but nothing in macaque or human testis (70). We show that MRP5 is detectable in the testes but that it also appears to be enriched in MAMs along with MRP9. Though MRP5 still localizes to basolateral plasma membranes in polarized MDCKII cells, our tissue fractionation studies bring to light the possibility of additional tissue-dependent expression patterns and subcellular localizations for this well-studied transporter. We envision that these results may have significant implications when it comes to cancer and the distinct roles MRPs may play dependent upon tissue/cell type. We propose the following model for the concerted function of MRP9 and MRP5 in the testes (Fig. 6*D*): In the absence of MRP9 and MRP5, metabolites, such as heme and/or other substrates, are inappropriately trafficked or distributed, causing mitochondrial damage. This dysfunction likely impacts signaling through EIF2 and mTOR pathways to regulate protein translation and UPR with corresponding changes in retinoic acid levels and signaling. Germ cells differentiate into mature spermatozoa, but these are functionally defective, as they fail to fertilize normal oocytes due to mitochondrial insufficiencies.

MRP9 is an enigmatic ABCC transporter. It has a unique expression pattern, no known drug substrates, and the last in the ABCC class still to be characterized (6, 24, 25). In the current study, we fill in some of the gaps in our knowledge by generating an MRP9 KO mouse model to explore its endogenous functions. We find that MRP9 is specifically expressed in developing spermatids and mature spermatozoa in mice, and unlike most other MRPs, MRP9 does not localize to the plasma membrane irrespective of cell polarization, consistent with the published findings of Ono et al. (24). Contrary to other reported studies, however, MRP9 is not endogenously expressed in any cell lines tested in our hands, including primary mouse embryonic fibroblasts, and MRP9 protein cannot be induced by sodium butyrate treatment (*SI Appendix*, Fig. S8), as was reported recently (71).

Transient transfections and tissue fractionations provide strong evidence that MRP9 partitions specifically to MAMs of the testes, a distinct compartment characterized by mitochondrial outer membrane and endoplasmic reticulum markers. This is physiologically reasonable, as MRP9 is localized to developing and mature spermatozoa, which are known to be devoid of traditional ER structures (72, 73). Though the ER is depleted in the process of differentiation, vestiges of ER membranes likely remain, particularly those in tight contact with mitochondria, and have been postulated to concentrate in the neck of the sperm midpiece to serve as a store for Ca^{2+} necessary for sperm activation (73, 74). Indeed, ER resident proteins such as ERp29 and Calreticulin have also been demonstrated to be present in sperm and play essential roles in acrosome reaction, fertilization, and stress responses (73, 74). We envision MRP9 may reside at these interfaces adjacent to mitochondria of the midpiece, effluxing substrates essential for regulating mitochondrial function and/or trafficking metabolites between these compartments as spermatogonia develop.

Loss of MRP9 alone has no discernable impact on male reproductive function, and KO mice are viable. Additionally, histological inspection of the testis and epididymis of these mice reveal effective spermatogenesis, with normal spermatid progression in seminiferous tubules and mature sperm in their convoluted ducts. Unsurprisingly, we also see no morphological defects evident by electron microscopy of sperm from MRP9 single KOs, as these male mice are perfectly capable of siring progeny even in a MRP5 heterozygous background. Any discernable impact on reproduction is only found when both MRP9 and MRP5 are ablated. Indeed, DKO mice show significant reproductive failures due to decreased male fecundity. Defects in sperm fertilization rates and high incidences of penile prolapse and seminal coagulum clogging contribute to their decrease in reproductive output as measured by litter size. This is likely due to the DKO sperm's inability to effectively fertilize, as supported by the drastically reduced IVF rates.

In addition to decreased motility trends, we show substantial changes in the composition of metabolites retained in the testes as well as significant perturbations in gene expression as a consequence of the loss of MRP9 and MRP5. Importantly, our integrative analysis of these approaches demonstrates that energy production and mitochondrial function were the most impacted pathways in the DKO testes, consistent with our localization studies. Targeted high-throughput metabolomics of subcellular fractions also revealed substantial changes at the subcellular level. While others have shown that triglyceride species can accumulate at the whole tissue level during mitochondrial dysfunction, we show that these lipid changes are occurring at the mitochondria and MAMs in the DKO testes (62, 63, 75, 76).

The top pathway identified by our gene expression analysis was EIF2 signaling, which we validated in vivo as a putative

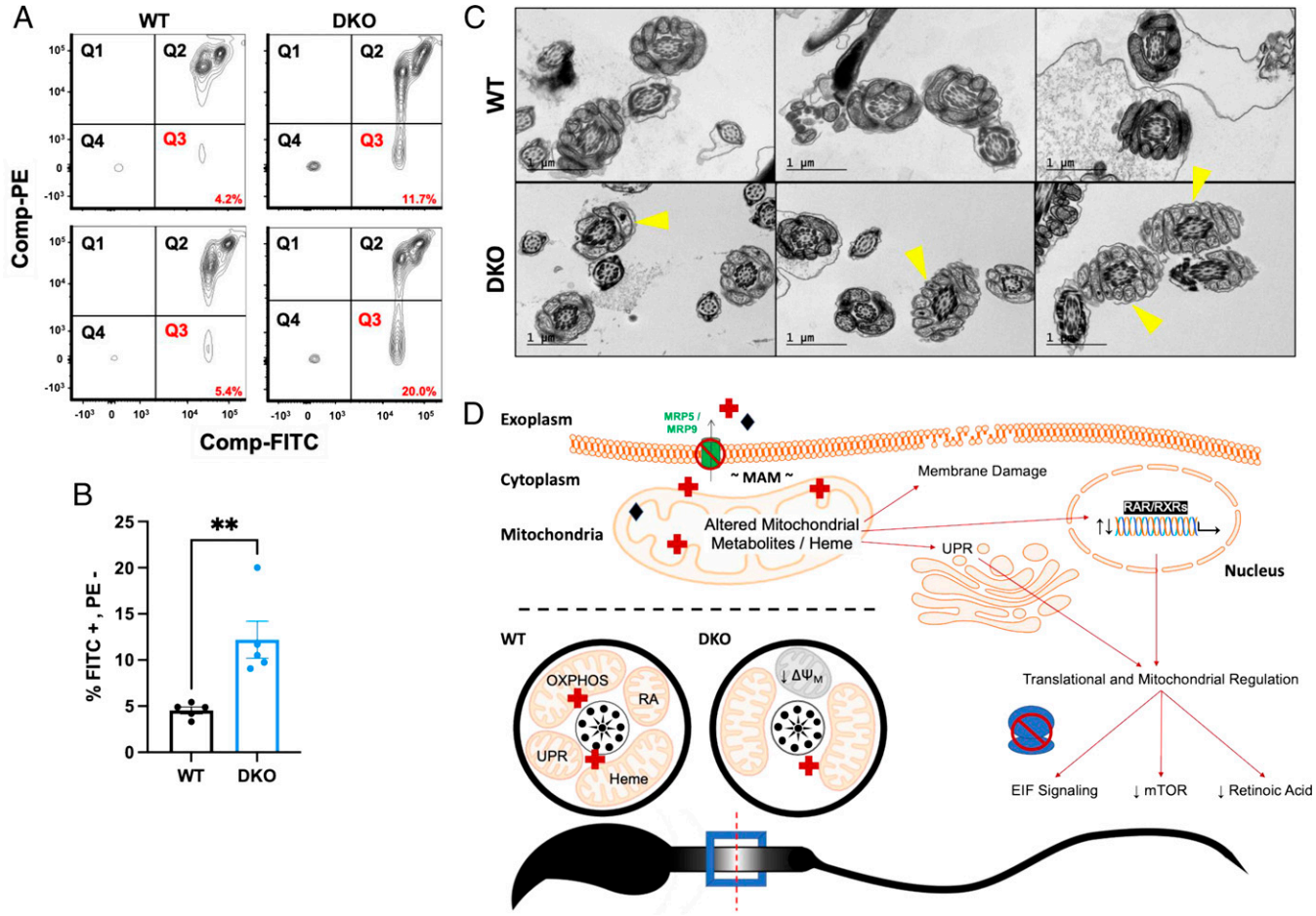

Fig. 6. Spermatozoa are severely compromised by the combined loss of MRP5 and MRP9. (*A*) Representative sorting analysis of two WT and DKO sperm samples stained with JC-1. Q3 is gating for populations that are FITC-pos and PE-neg representing a reduction J aggregates/red fluorescence and therefore decreased mitochondrial membrane potential. (*B*) Quantification of sperm stained with JC-1 and gated for populations that are FITC-pos and PE-neg (from *A*); $n = 5$ animals, $^{**}P$ value = 0.0055. (*C*) TEM of swum-out caudal epididymal spermatozoa from WT (*Top*) and DKO (*Bottom*). Cross sections of the sperm midpiece visualize cristae and mitochondrial morphology of the mitochondrial sheath. Yellow arrowheads highlight vacuolated and aberrant mitochondria. Representative images from at least 15 fields of view per sample. (Scale bar: 1 μm.) (*D*) Model figure: the combined ablation of MRP9 and MRP5 causes inappropriate trafficking or distribution of metabolites such as heme (red crosses) and/or other substrates (black diamonds) inducing mitochondrial damage. This dysfunction likely impacts signaling of the EIF2 and mTOR pathways to regulate protein translation and UPR with corresponding changes in retinoic acid levels and signaling. Germ cells differentiate into mature spermatozoa, but these are functionally defective as they fail to fertilize normal oocytes due to mitochondrial insufficiencies.

response to mitochondria dysfunction and/or possibly induced by alterations in heme levels in maturing sperm. Indeed, heme and iron-related genes were differentially expressed in the testes, and quantification of heme in the caudal epididymis of DKO mice showed significantly decreased levels. In a similar vein to the well-established models of UPR in the erythron, we envisage a necessity for heme sharing and partitioning, as mitochondria are rapidly being recruited and cells are undergoing proliferation for spermatogenesis and differentiation. Though this translational regulation via EIF2 signaling has been well studied in other contexts, virtually nothing is known about its role in the testes. The only published study to our knowledge relates to EIF2s3y, which was shown to be essential for regulating protein proliferation in spermatogenesis (77). It is yet to be determined whether or not this subunit plays any direct role to our findings here, although it is also significantly up-regulated in the DKO testes ($P = 0.022$).

Beyond EIF2 signaling, IPA identified several additional pathways: Protein Ubiquitination (essential for UPR), mTOR Signaling, Regulation of EIF4, Oxidative Phosphorylation, Germ Cell-Sertoli Cell Junction Signaling (an essential component of sperm differentiation), and Mitochondrial Dysfunction. It is plausible that all-*trans* retinoic acid may be a regulator in all these pathways for the following reasons: 1) it is essential in male fertility as one of the primary signaling molecules from Sertoli cells for progression of spermatogenesis; 2) it is critical for regulating gene expression of essential oxidative phosphorylation and mitochondrial genes; and 3) it has been shown to modulate mTOR and EIF4 regulation (51, 52, 57). Consistent with this notion, we find genes associated with retinoids and retinoic acid levels significantly decreased in DKO testes. Furthermore, targets of gene expression perturbation have significant enrichment of retinoic acid–related binding motifs for transcriptional regulation, albeit modulation via these motifs may be indirect. RORA has been reported to act as a constitutive activator of transcription in the absence of ligand, and all-*trans* retinoic acid does not bind to RXR with high affinity as compared to 9-*cis* retinoic acid (78, 79).

These systemic changes in the testes of DKO mice are in-line with the striking morphological abnormality of their mitochondria at the ultrastructural level. The impact of such evident dysfunction at the sperm midpiece has significant effects on male

fecundity. The mitochondrial sheath is essential for reproductive fitness, as these tightly wrapped mitochondria are critical for ATP production and maximizing efficiency of energy delivery, directly correlated with sperm swimming velocities across species (27, 28, 80–83). However, this immense output comes with a price—because spermatozoa are so densely packed with mitochondria, they are also epicenters for the production of detrimental free radicals/reactive oxygen species (27, 80, 82, 84). If not balanced and mitigated, this can cause myriads of problems, including lipid peroxidation, which has been shown to damage the sperm and decrease their mitochondrial membrane potential (27, 80, 82, 85). Loss of MRP5 and MRP9 alters mitochondrial homeostasis, not only inducing vacuolated and aberrant mitochondria but also resulting in a significant reduction in sperm mitochondrial membrane potential as observed by JC-1 staining. This relationship between mitochondrial membrane potential and sperm function directly correlates with mitochondrial health, sperm motility, and modulation of respiratory chain activity and oxidative phosphorylation pathways (27, 81, 86–88). Concordantly, male fecundity relies heavily on this organelle and its membranes being fully intact and functional for the overall health of the spermatozoa and their fertilization capacity, cementing why DKO males show such significant loss of biological function (27, 80–82). Male infertility is a significant problem globally, affecting over 70 million people and accounting for 50% of documented issues in infertile couples (81, 89, 90). To our knowledge, mutations or SNP variants of MRPs have not yet been investigated for any correlation to cases of male reproductive dysfunction. Our findings here would suggest that human patients with infertility issues, typically assayed for and characterized by mitochondrial dysfunctions, may have hypomorphic mutations in MRP9 and MRP5.

Materials and Methods

General Methods.

Animals. All mice used were housed in Animal Sciences Departmental facilities at the University of Maryland and kept in standard 12-h light-dark cycles. Both sexes were used for all experiments unless stipulated otherwise, such as the analysis of male sex organs and requisite male reproduction phenotypes. ABCC12/MRP9 mutant mice were generated via CRISPR/Cas9 RNA injections (*SI Appendix, Supplementary Materials and Methods*) at the National Human Genome Research Institute (NHGRI). MRP5 mutant mice, a gift from Dr. Piet Borst (Netherlands Cancer Institute), had previously been outcrossed into full C57BL/6 background and were bred to MRP9 mutant mice to generate DKOs. MRP5 and MRP9 mice were genotyped from tail genomic DNA via PCR and RFLP (restriction fragment length polymorphism) methods (*SI Appendix, Supplementary Materials and Methods* and Table S4). All subsequent protocols described as follows involving these animals were approved by the Institutional Animal Care and Use Committee at the University of Maryland, College Park.

Subcellular fractionation and MAM isolation. MAMs isolation and subcellular fractionizations were based off of Wieckowski et al. with minor modifications for optimization of testes tissue (32). Age-matched WT and DKO male mice were anesthetized with intraperitoneal injection of ketamine/xylene, and then systemic perfusion was performed via standard cardiac puncture method. Perfusion was performed with IB-1 buffer (225 mM mannitol, 75 mM sucrose, 0.5% bovine serum albumin [BSA], 0.5 mM ethylene glycol-bis(β-aminoethyl ether)-N,N,N′,N′-tetraacetic acid [EGTA], and 30 mM Tris–HCl pH 7.4) using 25 mL total pushed through a 30 mL syringe with a 26G needle (BD Precision Glide, cat. no. 305111) into the left ventricle of the beating heart, which upon completion resulted in completely cleared liver and kidneys. Livers and testes were then immediately harvested and placed in IB-3 buffer (225 mM mannitol, 75 mM sucrose, and 30 mM Tris–HCl pH 7.4) on ice at 4 °C, and the remaining isolation was performed entirely at 4 °C in a cold room. A single liver or four pooled testes were necessary to achieve sufficient yield of purified MAMs, which were minced and combined and then lysed in IB-1 buffer via 10 strokes in a 22 gauge 5 mL glass Duall Dounce homogenizer. The homogenate was then spun down twice at 740 × *g* to remove nuclei and cellular debris. The remaining supernatant was spun at 9,000 × *g* for the isolation of crude mitochondria, which was subsequently washed and spun down twice at 10,000 × *g*. The first 10,000 × *g* spin was in IB-2 buffer (225 mM mannitol, 75 mM sucrose, 0.16% BSA, and 30 mM Tris–HCl pH 7.4) and then the second in IB-3 for further purification prior to a 100,000 × *g* spin through a Percoll (Sigma, cat. no. P1644) gradient to separate MAMs from mitochondria. The original supernatant from the 9,000 × *g* spin was also spun down at 100,000 × *g* to concentrate the remaining smaller organelles, plasma membranes, and cytosolic proteins labeled "Membrane Prep." Each of the isolated fractions "740 × *g*," "Membrane Prep," "Mitochondria," and "MAMs" as well as total initial homogenate were subsequently lysed in lysis buffer and following standard immunoblotting methods (Supplementary Materials and Methods), ran side by side in a Criterion Precast Gradient 4 to 15% sodium dodecyl sulphate–polyacrylamide gel electrophoresis (SDS-PAGE) gel for Western blotting probing of key intracellular organellar markers and proteins of interest: HSP60 (Abcam, cat. no. ab46798), Calnexin (Abcam, cat. no. ab22595), Mitofusin 2 (Invitrogen 7H42L13, cat. no. 702768), MRP5, and MRP9.

Heme quantification. To extract heme from perfused mouse tissues, a minimum of 30 mg of caudal epididymides (either three or four pooled together), an entire testis, or seminal vesicle were Dounce homogenized fresh in a minimum of five volumes of lysis solution containing 50 mM Tris/HCl pH 8.0, 5 mM $CaCl_2$, 50 mM NaCl, 1% Triton X-100, and 0.5% Proteinase K. Proteinase K was added fresh to the buffer, and the homogenate was incubated overnight at 37 °C with moderate shaking. The next day, the Proteinase K digest was sonicated for 1 min (10 W, pulse 0.5 s) and centrifuged at 11,000 × *g* for 45 min, and then the supernatant was collected for heme quantification. The 20 μL of the tissue lysate sample was mixed with 180 μL of 2 M oxalic acid, and sample tubes were then heated in a water bath set at 100 °C for 30 min while a duplicate set of samples remain at room temperature as blank controls. Fluorescence of porphyrins were then read using Ex 400/10 nm, Em 645/40 nm on a BioTek microplate reader (BioTek, Synergy HT) and heme content calculated based off of a heme standard curve and subtraction of blank values (parallel unheated samples in oxalic acid) from samples.

Metabolomics Methods.

Global untargeted metabolomics of mouse testes. Tissue was first extracted either in aqueous or organic methods. For aqueous extractions, 10 volumes of methanol:H_2O (3:1) was added to the tissue sample and homogenized with ceramic beads (Precellys24-Dual, PeqLab). Then, 200 μL of the homogenate was transferred to a new tube where it was then vortexed and centrifuged at 15,000 rpm for 10 min at 4 °C. The supernatant was transferred to sample vial for ultra high performance liquid chromatography coupled with mass spectrometry (UHPLC-MS) analysis. Analytes were separated with either a CSH C18 column or a BEH amide column for more nonpolar and polar species, respectively. For the first aqueous method, separation was achieved using an ACQUITY UPLC CSH C18 Column (1.7 μm, 2.1 mm × 100 mm). Mobile phase A was water (contained 0.1% formic acid), and mobile phase B was acetonitrile (contained 0.1% formic acid). The gradient was 0 to 1 min, 5% B; 1.1 to 10 min, 5 to 95% B; 10.1 to 13 min, 95% B; 13.1 to 13.5 min, 95 to 5% B; 13.6 to 15 min, hold at 5% B. The flow rate was 0.5 mL/min. The column was maintained at 50 °C and the auto-sampler was kept at 10 °C. A 5 μL injection was used for all samples. For the second method of aqueous analysis, the separation was achieved using an ACQUITY UPLC BEH Amide Column (1.7 μm, 2.1 mm × 100 mm). Mobile phase A was water (contained 0.1% formic acid), and mobile phase B was acetonitrile (contained 0.1% formic acid). The gradient was 0 to 1 min, 99% B; 1 to 10 min, 99% to 30 B; 10.1 to 12 min, hold at 99% B. The flow rate was 0.5 mL/min. The column was maintained at 45 °C, and the auto-sampler was kept at 10 °C. A 5 μL injection was used for all samples. For both aqueous sample preps, data were acquired in both positive (HDMSe) and negative (HDMSe) mode. The capillary voltages were separated for positive (0.8 kV) and negative (0.8 kV) and sampling cone voltage was 40 V. Nitrogen at a flow of 800 L/h was used as the desolvation gas with a constant desolvation temperature of 500 °C. The source temperature was set at 150 °C. Data were acquired over the *m/z* range of 50 to 1,000. For organic extraction (lipid) methods, likewise, 10 volumes of methanol:H_2O (3:1) was added to the tissue sample and homogenized with ceramic beads (Precellys24-Dual, PeqLab). However, now after homogenization, 400 μL was transferred to a new tube and 500 μL of ice-cold methyl-tert-butyl ether is added, prior to incubation at 650 rpm for 1 h. Additionally, 500 μL of ice-cold water was then added and incubated at 650 rpm for 15 min before phase separation was completed by centrifugation for 8 min at 8,000 rpm at 4 °C. The top (organic) layer was removed and dried at room temperature under nitrogen. The recovered lipids were reconstituted in 200 μL of isopropanol:acetonitrile:water (2:1:1, vol/vol/v) and were transferred to sample vial for UHPLC-MS analysis. The separation was achieved using a CORTECS HILIC Column (2.7 μm, 2.1 mm × 100 mm). Mobile phase A was water/acetonitrile (5:95, vol/vol) with 10 mM ammonium acetate and mobile phase B water/acetonitrile (50:50, vol/vol) with 10 mM ammonium acetate. The gradient was ramped from 0.1 to 20% B in 10 min, ramped to 80% B in 3 min, ramped back down to 0.1% B and held for 3 min.

The flow rate was 0.5 mL/min. The column was maintained at 30 °C and the auto-sampler was kept at 10 °C. A 5 μL injection was used for all samples. Like the aqueous phase, data were acquired in both positive (HDMSe) and negative (HDMSe) mode. The capillary voltages were separated for positive (2.8 kV) and negative (1.9 kV) and sampling cone voltage was 30 V. Nitrogen at a flow of 900 L/h was used as the desolvation gas with a constant desolvation temperature of 550 °C. The source temperature was set at 120 °C. Data were acquired over the *m/z* range of 100 to 1,500. Positive and negative mode data were basally analyzed by Progenesis QI, and putative metabolite identification was searched by using HMDB and LIPID MAPS databases (delta < 5 ppm). The output marker lists were then manually sorted and annotated for more sophisticated downstream analysis with MetaboAnalyst (91–93). Multivariate data analysis, volcano plots, Variable Importance in Projection (VIP) heatmaps, and mummichog algorithm analysis to putatively annotate metabolites were performed using MetaboAnalyst 4.0 (35).

Transcriptomics and Associated Methods.

RNAseq of mouse testes. RNA was extracted from frozen tissues following standard TRIzol chloroform protocol (Invitrogen, cat. no. 15596026), and aqueous fractions were then taken directly into Qiagen RNA plus extraction kit (Qiagen, cat. no. 74136) for maximum purity. Total RNA quality and quantity were tested on an Agilent Bioanalyzer 2100 System (Agilent cat. no. G2939BA) using RNA Nano Chip On-Chip Electrophoresis trays for samples with RNA integrity number scores greater than 8 prior to processing for library prep/construction and sequencing. RNAseq was performed at NIH Intramural Sequencing Center (NISC) using Illumina NovaSeq 6000. FastQC, version 0.11.7, was used as an additional bioinformatics quality control on output reads from sequencing. The reads were then aligned to the mouse mm10 GRCh38 reference genome for gene annotation using STAR (Spliced Transcripts Alignment to a Reference), version 2.7.0f, and numbers of reads in transcripts per million (TPM) mapped to genes were counted generating matrixes for all samples. Differentially expressed genes were then identified via both manual export, sorting and fold change annotation, as well as processed via DESeq2, version 1.12.3, for more complex analysis. DESeq2 was run using R (version 3.6.1) and Bioconductor (version 3.4) with BioInstaller (version 1.24.0) for volcano plotting and statistical analysis of differential changes utilizing adjusted P value < 0.01 and false discovery rate cutoffs of 0.05. The complete RNAseq results have been depositing to the National Center for Biotechnology Information (NCBI) Gene Expression Omnibus under accession number GSE176740 (94).

Additional Bioinformatics and Statistical Analyses. All alignment and evolutionary analyses were conducted using MEGA X software version 10.2.4 (95–98). All data throughout are expressed as means ± SEM unless otherwise stated. Means of groups were assessed by using two-sided, unpaired Student's *t* test or the equivalent analyses where applicable unless otherwise stated. A P value of <0.05 when compared to baseline values or genotypes (WT) was considered statistically significant. All analyses were performed using Prism 9 software (GraphPad, version 9.1.0).

Data Availability. RNAseq data have been deposited in NCBI Gene Expression Omnibus (GSE176740) (94).

ACKNOWLEDGMENTS. We would like to acknowledge Ms. Lisa Garrett for conducting the pronuclear injections at NHGRI, NIH to generate the *Abcc12* mouse. We also thank Mr. Simon Beardsley for sharing the *C. elegans mrp-5* data. We acknowledge the Imaging Core Facility in the Department of Cell Biology and Molecular Genetics at the University of Maryland, College Park, supported by Award No. 1S10OD025223-01A1 from NIH. This work was also done in part by utilizing the computational resources of the NIH High Performance Computing Biowulf cluster (https://hpc.nih.gov). The MRP5 (M5I-10, M5-NC3) and MRP9 (M9I-27, M9I-38, M9II-3) antibodies used throughout were a generous gift from Piet Borst/Koen van de Wetering (Netherlands Cancer Institute). This work was supported by funding from NIH DK85035 and DK125740 (I.H.) and HD077260 (M.A.K.); the Utah Center for Iron and Heme Disorders was supported by funding from DK110858 (J.D.P.); and the Intramural Program of the NHGRI (D.B.). The funders had no role in study design, data collection and analysis, decision to publish, or preparation of the manuscript.

1. M. Kool *et al.*, Analysis of expression of cMOAT (MRP2), MRP3, MRP4, and MRP5, homologues of the multidrug resistance-associated protein gene (MRP1), in human cancer cell lines. *Cancer Res.* **57**, 3537–3547 (1997).
2. M. A. McAleer, M. A. Breen, N. L. White, N. Matthews, pABC11 (also known as MOAT-C and MRP5), a member of the ABC family of proteins, has anion transporter activity but does not confer multidrug resistance when overexpressed in human embryonic kidney 293 cells. *J. Biol. Chem.* **274**, 23541–23548 (1999).
3. P. Borst, R. Evers, M. Kool, J. Wijnholds, A family of drug transporters: The multidrug resistance-associated proteins. *J. Natl. Cancer Inst.* **92**, 1295–1302 (2000).
4. G. D. Kruh, M. G. Belinsky, The MRP family of drug efflux pumps. *Oncogene* **22**, 7537–7552 (2003).
5. P. M. Jones, A. M. George, The ABC transporter structure and mechanism: Perspectives on recent research. *Cell. Mol. Life Sci.* **61**, 682–699 (2004).
6. A. J. Slot, S. V. Molinski, S. P. Cole, Mammalian multidrug-resistance proteins (MRPs). *Essays Biochem.* **50**, 179–207 (2011).
7. J.-Y. Lee, D. M. Rosenbaum, Transporters revealed. *Cell* **168**, 951–953 (2017).
8. B. Sarkadi, M. Müller, Z. Holló, The multidrug transporters–Proteins of an ancient immune system. *Immunol. Lett.* **54**, 215–219 (1996).
9. I. B. Holland, M. A. Blight, ABC-ATPases, adaptable energy generators fuelling transmembrane movement of a variety of molecules in organisms from bacteria to humans. *J. Mol. Biol.* **293**, 381–399 (1999).
10. S. P. Cole *et al.*, Overexpression of a transporter gene in a multidrug-resistant human lung cancer cell line. *Science* **258**, 1650–1654 (1992).
11. S. P. C. Cole, Targeting multidrug resistance protein 1 (MRP1, ABCC1): Past, present, and future. *Annu. Rev. Pharmacol. Toxicol.* **54**, 95–117 (2014).
12. C. A. Ritter *et al.*, Cellular export of drugs and signaling molecules by the ATP-binding cassette transporters MRP4 (ABCC4) and MRP5 (ABCC5). *Drug Metab. Rev.* **37**, 253–278 (2005).
13. R. G. Deeley, C. Westlake, S. P. Cole, Transmembrane transport of endo- and xenobiotics by mammalian ATP-binding cassette multidrug resistance proteins. *Physiol. Rev.* **86**, 849–899 (2006).
14. T. Korolnek, J. Zhang, S. Beardsley, G. L. Scheffer, I. Hamza, Control of metazoan heme homeostasis by a conserved multidrug resistance protein. *Cell Metab.* **19**, 1008–1019 (2014).
15. G. Jedlitschky, B. Burchell, D. Keppler, The multidrug resistance protein 5 functions as an ATP-dependent export pump for cyclic nucleotides. *J. Biol. Chem.* **275**, 30069–30074 (2000).
16. G. Reid *et al.*, Characterization of the transport of nucleoside analog drugs by the human multidrug resistance proteins MRP4 and MRP5. *Mol. Pharmacol.* **63**, 1094–1103 (2003).
17. R. S. Jansen, S. Mahakena, M. de Haas, P. Borst, K. van de Wetering, ATP-binding cassette subfamily C member 5 (ABCC5) functions as an efflux transporter of glutamate conjugates and analogs. *J. Biol. Chem.* **290**, 30429–30440 (2015).
18. X. Yuan *et al.*, Regulation of intracellular heme trafficking revealed by subcellular reporters. *Proc. Natl. Acad. Sci. U.S.A.* **113**, E5144–E5152 (2016).
19. R. K. Donegan, C. M. Moore, D. A. Hanna, A. R. Reddi, Handling heme: The mechanisms underlying the movement of heme within and between cells. *Free Radic. Biol. Med.* **133**, 88–100 (2019).
20. I. G. Chambers, M. M. Willoughby, I. Hamza, A. R. Reddi, One ring to bring them all and in the darkness bind them: The trafficking of heme without deliverers. *Biochim. Biophys. Acta Mol. Cell Res.* **1868**, 118881 (2021).
21. A. R. Reddi, I. Hamza, Heme mobilization in animals: A metallolipid's journey. *Acc. Chem. Res.* **49**, 1104–1110 (2016).
22. J. Tammur *et al.*, Two new genes from the human ATP-binding cassette transporter superfamily, ABCC11 and ABCC12, tandemly duplicated on chromosome 16q12. *Gene* **273**, 89–96 (2001).
23. T. K. Bera *et al.*, MRP9, an unusual truncated member of the ABC transporter superfamily, is highly expressed in breast cancer. *Proc. Natl. Acad. Sci. U.S.A.* **99**, 6997–7002 (2002).
24. N. Ono *et al.*, Multidrug resistance-associated protein 9 (ABCC12) is present in mouse and boar sperm. *Biochem. J.* **406**, 31–40 (2007).
25. H. Shimizu *et al.*, Characterization of the mouse Abcc12 gene and its transcript encoding an ATP-binding cassette transporter, an orthologue of human ABCC12. *Gene* **310**, 17–28 (2003).
26. M. Jung *et al.*, Unified single-cell analysis of testis gene regulation and pathology in five mouse strains. *eLife* **8**, e43966 (2019).
27. A. Amaral, B. Lourenço, M. Marques, J. Ramalho-Santos, Mitochondria functionality and sperm quality. *Reproduction* **146**, R163–R174 (2013).
28. N.-H. Gu, W.-L. Zhao, G.-S. Wang, F. Sun, Comparative analysis of mammalian sperm ultrastructure reveals relationships between sperm morphology, mitochondrial functions and motility. *Reprod. Biol. Endocrinol.* **17**, 66 (2019).
29. D. Stojanovski, M. Bohnert, N. Pfanner, M. van der Laan, Mechanisms of protein sorting in mitochondria. *Cold Spring Harb. Perspect. Biol.* **4**, a011320 (2012).
30. J. Lee, D. H. Kim, I. Hwang, Specific targeting of proteins to outer envelope membranes of endosymbiotic organelles, chloroplasts, and mitochondria. *Front Plant Sci* **5**, 173 (2014).
31. J. E. Vance, MAM (mitochondria-associated membranes) in mammalian cells: Lipids and beyond. *Biochim. Biophys. Acta* **1841**, 595–609 (2014).
32. M. R. Wieckowski, C. Giorgi, M. Lebiedzinska, J. Duszynski, P. Pinton, Isolation of mitochondria-associated membranes and mitochondria from animal tissues and cells. *Nat. Protoc.* **4**, 1582–1590 (2009).
33. P. Pinton, Mitochondria-associated membranes (MAMs) and pathologies. *Cell Death Dis.* **9**, 413 (2018).
34. M. Yang *et al.*, Mitochondria-associated ER membranes - The origin site of autophagy. *Front. Cell Dev. Biol.* **8**, 595 (2020).
35. S. Li *et al.*, Predicting network activity from high throughput metabolomics. *PLOS Comput. Biol.* **9**, e1003123 (2013).

36. D. Phillips, A. M. Aponte, S. A. French, D. J. Chess, R. S. Balaban, Succinyl-CoA synthetase is a phosphate target for the activation of mitochondrial metabolism. *Biochemistry* **48**, 7140–7149 (2009).
37. I. Martínez-Reyes, N. S. Chandel, Mitochondrial TCA cycle metabolites control physiology and disease. *Nat. Commun.* **11**, 102 (2020).
38. J. J. Chen, S. Zhang, Heme-regulated eIF2α kinase in erythropoiesis and hemoglobinopathies. *Blood* **134**, 1697–1707 (2019).
39. A. P. Han *et al.*, Heme-regulated eIF2alpha kinase (HRI) is required for translational regulation and survival of erythroid precursors in iron deficiency. *EMBO J.* **20**, 6909–6918 (2001).
40. J. Igarashi *et al.*, Elucidation of the heme binding site of heme-regulated eukaryotic initiation factor 2α kinase and the role of the regulatory motif in heme sensing by spectroscopic and catalytic studies of mutant proteins. *J. Biol. Chem.* **283**, 18782–18791 (2008).
41. R. N. V. S. Suragani *et al.*, Heme-regulated eIF2α kinase activated Atf4 signaling pathway in oxidative stress and erythropoiesis. *Blood* **119**, 5276–5284 (2012).
42. H. Mellor, K. M. Flowers, S. R. Kimball, L. S. Jefferson, Cloning and characterization of cDNA encoding rat hemin-sensitive initiation factor-2 alpha (eIF-2 alpha) kinase. Evidence for multitissue expression. *J. Biol. Chem.* **269**, 10201–10204 (1994).
43. J. J. Berlanga, S. Herrero, C. de Haro, Characterization of the hemin-sensitive eukaryotic initiation factor 2α kinase from mouse nonerythroid cells. *J. Biol. Chem.* **273**, 32340–32346 (1998).
44. A. B. Page *et al.*, Persistent eIF2alpha(P) is colocalized with cytoplasmic cytochrome c in vulnerable hippocampal neurons after 4 hours of reperfusion following 10-minute complete brain ischemia. *Acta Neuropathol.* **106**, 8–16 (2003).
45. T. Tsuyama, A. Tsubouchi, T. Usui, H. Imamura, T. Uemura, Mitochondrial dysfunction induces dendritic loss via eIF2α phosphorylation. *J. Cell Biol.* **216**, 815–834 (2017).
46. S. Zhang *et al.*, HRI coordinates translation necessary for protein homeostasis and mitochondrial function in erythropoiesis. *eLife* **8**, e46976 (2019).
47. Y. Miyagi *et al.*, Abundant expression of translation initiation factor EIF-4E in postmeiotic germ cells of the rat testis. *Lab. Invest.* **73**, 890–898 (1995).
48. J. Marill, N. Idres, C. C. Capron, E. Nguyen, G. G. Chabot, Retinoic acid metabolism and mechanism of action: A review. *Curr. Drug Metab.* **4**, 1–10 (2003).
49. N. Y. Kedishvili, Enzymology of retinoic acid biosynthesis and degradation: Thematic review series: Fat-soluble vitamins: Vitamin A. *J. Lipid Res.* **54**, 1744–1760 (2013).
50. T. J. Cunningham, G. Duester, Mechanisms of retinoic acid signalling and its roles in organ and limb development. *Nat. Rev. Mol. Cell Biol.* **16**, 110–123 (2015).
51. H. B. Everts, C. D. Berdanier, Regulation of mitochondrial gene expression by retinoids. *IUBMB Life* **54**, 45–49 (2002).
52. R. Puttagunta, S. Di Giovanni, Retinoic acid signaling in axonal regeneration. *Front. Mol. Neurosci.* **4**, 59 (2012).
53. C. D. Berdanier, H. B. Everts, C. Hermoyian, C. E. Mathews, Role of vitamin A in mitochondrial gene expression. *Diabetes Res. Clin. Pract.* **54** (suppl. 2), S11–S27 (2001).
54. N. Noy, Retinoid-binding proteins: Mediators of retinoid action. *Biochem. J.* **348**, 481–495 (2000).
55. J. L. Napoli, Cellular retinoid binding-proteins, CRBP, CRABP, FABP5: Effects on retinoid metabolism, function and related diseases. *Pharmacol. Ther.* **173**, 19–33 (2017).
56. R.-Z. Liu *et al.*, CRABP1 is associated with a poor prognosis in breast cancer: Adding to the complexity of breast cancer cell response to retinoic acid. *Mol. Cancer* **14**, 129 (2015).
57. C. A. Hogarth, M. D. Griswold, The key role of vitamin A in spermatogenesis. *J. Clin. Invest.* **120**, 956–962 (2010).
58. J. K. Amory *et al.*, Isotretinoin administration improves sperm production in men with infertility from oligoasthenozoospermia: A pilot study. *Andrology* **5**, 1115–1123 (2017).
59. J. T. Busada *et al.*, Retinoic acid regulates Kit translation during spermatogonial differentiation in the mouse. *Dev. Biol.* **397**, 140–149 (2015).
60. M. D. Griswold, Spermatogenesis: The commitment to meiosis. *Physiol. Rev.* **96**, 1–17 (2016).
61. C. Peluso-Iltis, J. Osz, N. Rochel, "DNA recognition by retinoic acid nuclear receptors" in *Methods in Enzymology*, E. Pohl, Ed. (Elsevier, 2020), pp. 235–260.
62. S. Vankoningsloo *et al.*, Mitochondrial dysfunction induces triglyceride accumulation in 3T3-L1 cells: Role of fatty acid beta-oxidation and glucose. *J. Lipid Res.* **46**, 1133–1149 (2005).
63. Y. Kawano, D. E. Cohen, Mechanisms of hepatic triglyceride accumulation in non-alcoholic fatty liver disease. *J. Gastroenterol.* **48**, 434–441 (2013).
64. Y. Toyoda *et al.*, MRP class of human ATP binding cassette (ABC) transporters: Historical background and new research directions. *Xenobiotica* **38**, 833–862 (2008).
65. Y. K. Zhang, Y. J. Wang, P. Gupta, Z. S. Chen, Multidrug resistance proteins (MRPs) and cancer therapy. *AAPS J.* **17**, 802–812 (2015).
66. A. Lorico *et al.*, Disruption of the murine MRP (multidrug resistance protein) gene leads to increased sensitivity to etoposide (VP-16) and increased levels of glutathione. *Cancer Res.* **57**, 5238–5242 (1997).
67. J. Wijnholds *et al.*, Increased sensitivity to anticancer drugs and decreased inflammatory response in mice lacking the multidrug resistance-associated protein. *Nat. Med.* **3**, 1275–1279 (1997).
68. C. J. F. de Wolf *et al.*, cGMP transport by vesicles from human and mouse erythrocytes. *FEBS J.* **274**, 439–450 (2007).
69. P. Borst, C. de Wolf, K. van de Wetering, Multidrug resistance-associated proteins 3, 4, and 5. *Pflugers Arch.* **453**, 661–673 (2007).
70. D. M. Klein, S. H. Wright, N. J. Cherrington, Localization of multidrug resistance-associated proteins along the blood-testis barrier in rat, macaque, and human testis. *Drug Metab. Dispos.* **42**, 89–93 (2014).
71. B. Shi *et al.*, Effect of sodium butyrate on ABC transporters in lung cancer A549 and colorectal cancer HCT116 cells. *Oncol. Lett.* **20**, 148 (2020).
72. S. Costello *et al.*, Ca2+-stores in sperm: Their identities and functions. *Reproduction* **138**, 425–437 (2009).
73. K. K. Karna, Y. S. Shin, B. R. Choi, H. K. Kim, J. K. Park, The role of endoplasmic reticulum stress response in male reproductive physiology and pathology: A review. *World J. Mens Health* **38**, 484–494 (2020).
74. X. Ying *et al.*, Endoplasmic reticulum protein 29 (ERp29), a protein related to sperm maturation is involved in sperm-oocyte fusion in mouse. *Reprod. Biol. Endocrinol.* **8**, 10 (2010).
75. T. Klopstock *et al.*, Mitochondrial DNA mutations in multiple symmetric lipomatosis. *Mol. Cell. Biochem.* **174**, 271–275 (1997).
76. A. Muñoz-Málaga *et al.*, Lipomatosis, proximal myopathy, and the mitochondrial 8344 mutation. A lipid storage myopathy? *Muscle Nerve* **23**, 538–542 (2000).
77. S. Mazeyrat *et al.*, A Y-encoded subunit of the translation initiation factor Eif2 is essential for mouse spermatogenesis. *Nat. Genet.* **29**, 49–53 (2001).
78. J. M. Harris, P. Lau, S. L. Chen, G. E. Muscat, Characterization of the retinoid orphan-related receptor-alpha coactivator binding interface: A structural basis for ligand-independent transcription. *Mol. Endocrinol.* **16**, 998–1012 (2002).
79. G. Allenby *et al.*, Retinoic acid receptors and retinoid X receptors: Interactions with endogenous retinoic acids. *Proc. Natl. Acad. Sci. U.S.A.* **90**, 30–34 (1993).
80. N. Srivastava, M. Pande, Mitochondrion: Features, functions and comparative analysis of specific probes in detecting sperm cell damages. *Asian Pac. J. Reprod.* **5**, 445–452 (2016).
81. K. Nowicka-Bauer *et al.*, Sperm mitochondrial dysfunction and oxidative stress as possible reasons for isolated asthenozoospermia. *J. Physiol. Pharmacol.* **69**, 403–417 (2018).
82. J. D. A. Losano *et al.*, Spermatic mitochondria: Role in oxidative homeostasis, sperm function and possible tools for their assessment. *Zygote* **26**, 251–260 (2018).
83. G. E. Olson, V. P. Winfrey, Structural organization of surface domains of sperm mitochondria. *Mol. Reprod. Dev.* **33**, 89–98 (1992).
84. M. Maneesh, H. Jayalekshmi, Role of reactive oxygen species and antioxidants on pathophysiology of male reproduction. *Indian J. Clin. Biochem.* **21**, 80–89 (2006).
85. A. J. Koppers, L. A. Mitchell, P. Wang, M. Lin, R. J. Aitken, Phosphoinositide 3-kinase signalling pathway involvement in a truncated apoptotic cascade associated with motility loss and oxidative DNA damage in human spermatozoa. *Biochem. J.* **436**, 687–698 (2011).
86. A. Amaral, J. Ramalho-Santos, Assessment of mitochondrial potential: Implications for the correct monitoring of human sperm function. *Int. J. Androl.* **33**, e180–e186 (2010).
87. A. Amaral *et al.*, Identification of proteins involved in human sperm motility using high-throughput differential proteomics. *J. Proteome Res.* **13**, 5670–5684 (2014).
88. A. Alamo *et al.*, Mitochondrial membrane potential predicts 4-hour sperm motility. *Biomedicines* **8**, 196 (2020).
89. K. Hwang, R. C. Walters, L. I. Lipshultz, Contemporary concepts in the evaluation and management of male infertility. *Nat. Rev. Urol.* **8**, 86–94 (2011).
90. J. Fainberg, J. A. Kashanian, Recent advances in understanding and managing male infertility. *F1000 Res.* **8**, F1000 Faculty Rev-670 (2019).
91. J. Chong *et al.*, MetaboAnalyst 4.0: Towards more transparent and integrative metabolomics analysis. *Nucleic Acids Res.* **46** (W1), W486–W494 (2018).
92. J. Chong, M. Yamamoto, J. Xia, MetaboAnalystR 2.0: From raw spectra to biological insights. *Metabolites* **9**, 57 (2019).
93. J. Chong, D. S. Wishart, J. Xia, Using metaboanalyst 4.0 for comprehensive and integrative metabolomics data analysis. *Curr. Protoc. Bioinformatics* **68**, e86 (2019).
94. I. Chambers *et al.*, MRP5 and MRP9 Play a Concerted Role in Male Reproduction and Mitochondrial Function. NCBI Gene Expression Omnibus. https://www.ncbi.nlm.nih.gov/geo/query/acc.cgi?acc=GSE176740. Deposited 10 June 2021.
95. N. Saitou, M. Nei, The neighbor-joining method: A new method for reconstructing phylogenetic trees. *Mol. Biol. Evol.* **4**, 406–425 (1987).
96. E. Zuckerkandl, L. Pauling, "Evolutionary divergence and convergence in proteins" in *Evolving Genes and Proteins*, V. Bryson, H. J. Vogel, Eds. (Academic Press, 1965), pp. 97–166.
97. S. Kumar, G. Stecher, M. Li, C. Knyaz, K. Tamura, MEGA X: Molecular evolutionary genetics analysis across computing platforms. *Mol. Biol. Evol.* **35**, 1547–1549 (2018).
98. G. Stecher, K. Tamura, S. Kumar, Molecular evolutionary genetics analysis (MEGA) for macOS. *Mol. Biol. Evol.* **37**, 1237–1239 (2020).